



RESEARCH ARTICLE

ROLE of Pt, Cu, Au and Cr UNDERLAYERS on EXCHANGE BIAS PROPERTIES in Pt/Py/IrMn THIN FILMS

Mustafa ÖZTÜRK^{1*}

^{1*}Gebze Technical University, Department of Physics, Gebze, mozturk@gtu.edu.tr, ORCID: 0000-0002-4564-3435

Receive Date: 19.07.2022

Accepted Date: 16.08.2022

ABSTRACT

Herein, the structural and magnetic properties of polycrystalline UL-X/Pt/Py/IrMn thin films were studied to observe the role of an underlayer on the exchange bias properties. Thin films with Pt, Cu, Au or Cr underlayers (UL-X) were deposited at room temperature by magnetron sputtering. The structural properties of the samples were investigated to analyze the layer thicknesses, material densities, interface roughnesses, and crystal structures of the samples. Magnetic characterization measurements were performed to obtain the sign and the value of exchange bias properties in the samples. The differences in the sign and the value of exchange bias effect in the samples with different underlayers are mainly explained by discussing the effects of lattice parameters and growth conditions. On this basis, one would expect that these results will help in designing new spintronic devices.

Keywords: *Magnetic multilayers, exchange bias, buffer layer, underlayer*

1. INTRODUCTION

Ultrathin magnetic multilayers are elementary units in spintronics applications such as magnetic random-access memories (MRAM), magnetic data storage devices, and magnetic sensors [1, 2]. For these spintronic applications, the need for reliable, energy-efficient, robust, faster, versatile, rugged, smaller, and non-volatile devices makes the wise design of multilayers more important.

Exchange bias (EB) is defined as the shift of hysteresis loops of a ferromagnetic (FM) layer when it is in close contact with an antiferromagnetic (AF) layer [3]. In the research field of magnetic multilayers, exchange-biased thin films with FM/AF layers have recently taken much notice [4-10]. Because the coercive field (H_C) values and the shift of hysteresis loops in FM layers can easily be adjusted with structural changes [11, 12] with the help of the EB effect. In recent years, several works have reported the interaction between the electrical current and the exchange-biased multilayers [4-7]. The value and the direction of the EB effect are very important for such kinds of work. Current or voltage interaction with EB is remarkable because the magnetization can be controlled with low energy consumption for highly efficient new generation devices through the current or voltage instead of the external magnetic field [6]. Particularly, spin-orbit torque (SOT) is a promising method for switching the magnetic properties in exchange-biased multilayers since SOT is generated simply by passing an electric current through a heavy metal (HM) [5-7, 13-20]. The SOT method can be applied

in EB structures as HM/FM/AF multilayers [6, 7, 21]. In such methods, the effective field can strongly depend on the chosen HM layer, e.g., the usage of Ta or Pt can differ the sign of spin Hall angle in the multilayers [22]. Apart from the HM, when creating a sample stack for such studies, a layer that is called an underlayer (UL) (or seed layer or buffer layer) can be placed between the substrate and the HM. The underlayers are used for reasons such as strengthening the crystal structure of the system, ensuring good adhesion of the thin film to the substrate, or reducing the roughness between the subsequent surfaces [12, 23]. Indeed, a UL can play a vital role in the stack by strongly affecting not only the structural properties but also the magnetic properties [23-26].

In this paper, we analyze how the H_C and exchange bias field (H_{EB}) parameters can be adjusted in principle by varying the UL material under the HM/FM/AF stacks. The contribution of UL to the magnetic properties was investigated by growing Pt, Cu, Au or Cr ULs under the sample systems consisting of exchange-biased Pt/Py/IrMn multilayers. The first Pt in the stack is designed as an HM but its usage as a UL is also analyzed. Our results with different ULs suggest that exchange bias properties at the interface of FM/AF can be modified considerably through UL engineering, which has a not to be underestimated indirect effect of UL on the interface of FM and AF layers.

2. EXPERIMENTAL DETAIL

In this article, four polycrystalline thin films with UL-X (5 nm)/ Pt (8 nm)/ Py(6 nm)/ IrMn(12 nm)/ Pt(3 nm) layers were grown on top of Si/SiO₂ substrates, as given in figure 1a, by using a six-gun sputtering chamber. The dimensions of the used substrates were $5 \times 10 \times 0.5$ mm. The difference between the four samples was their ULs which were used between the substrates and HM. A 5nm of Pt, Au, Cu or Cr layer was chosen as a UL-x in the stacks. It is aimed to make comparisons between their functionalities as a UL for an exchange-biased magnetic multilayer. To define the samples in the article easily, they are shortly named by using their UL types as UL-Pt, UL-Au, UL-Cu and UL-Cr. The additional presence of 8 nm Pt after the UL-Xs in all samples is because Pt typically promotes in-plane anisotropy during the growth of the FM layer [22]. The top Pt capping layers are used in the stacks to protect the stacks from outer oxidation.

Ferromagnetic Py and antiferromagnetic IrMn in the study were grown from Ni₈₀Fe₂₀ and Ir₂₂Mn₇₈ alloyed targets, respectively. The thickness values of both Py and IrMn were chosen after several preliminary trials until a significant EB effect was observed at RT. Then the samples of this study were grown with these nominal values. IrMn has a Néel temperature much higher than the RT [27, 28]. This helps to provide good magnetic and thermal stability during the exchange interaction of FM/AF.

The top schematic view drawing of the substrate position and the relative target gun positions in the sputter chamber was given in figure 1b. During the depositions, the substrate positions to the targets has been kept constant, and their long sides were perpendicular to the projection of the growth direction of Py.

The base pressure of the chamber was about 10^{-8} mbar before the depositions of each sample. During the sputtering, Ar pressure was kept around 10^{-3} mbar. To avoid any thermal interdiffusion at the FM/AF interface, samples were deposited at RT.

For the structural characterization of the samples, X-Ray Reflectivity (XRR) and X-ray diffraction (XRD) measurements have been performed by Rigaku Smartlab and Bruker D8 Advance X-Ray diffractometers, respectively. The magnetic properties of the samples were recorded by using a homemade magneto-optical Kerr effect (MOKE) measurement setup [29]. This homemade MOKE system consists of a He-Ne laser with a wavelength of 632.8 nm and an electromagnet that applies magnetic fields up to 1.6 Tesla. During MOKE measurements, the applied magnetic field angle was varied along the film plane. The azimuthal angle (Φ_H) given in figure 1c has been varied but the polar angle (Θ_H) has always been kept constant. This measurement geometry corresponds to the so-called longitudinal MOKE (LMOKE) geometry. Here, the angle $\Phi_H=0^\circ$ was determined before the sample growth with the expectation that the easy axis of the ferromagnetic layer is parallel to the long side of the samples. All magnetic measurements of this article are performed at RT. Layer thicknesses of the samples were controlled by the deposition time after having a careful growth rate calibration. The growth rate was determined as a result of the analysis of the XRR measurements of thick preliminary samples prepared before this study.

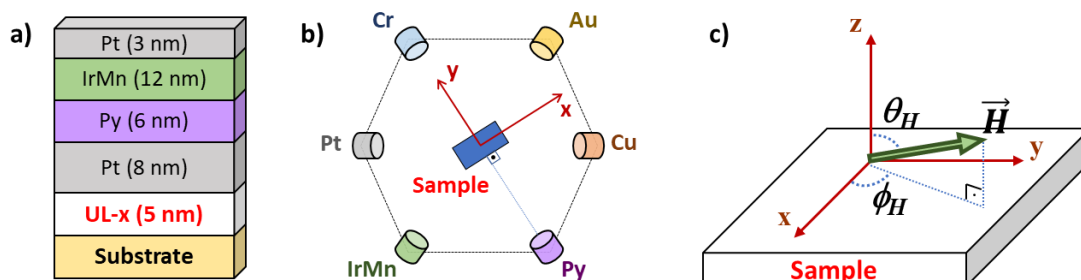


Figure 1. Schematic drawing of (a) the grown sample stack, (b) the gun positions in the sputter chamber and (c) magnetic property measurement geometry of samples. Here in (c), \vec{H} defines the applied magnetic field to the sample and Φ_H defines the angle that the xy projection of the applied magnetic field makes with the x -axis.

3. RESULTS AND DISCUSSION

Figure 2a shows the XRD patterns of the polycrystalline samples. From the XRD patterns, the peaks at $2\Theta = 39.8^\circ$ and 38.1° can be attributed to Pt (111) and Au (111) textures, respectively. From the XRD patterns in figure 2a, it can be seen that all the samples show a remarkable fcc Pt (111) texture. Almost all Pt (111) peaks are shifted compared to the bulk materials, which are thought to result from mechanically induced strain during deposition. The lattice constant of a bulk Pt (111) reflection is known as 3.92 \AA . The calculated lattice constant from the Pt (111) layers is found $3.90 \pm 0.01 \text{ \AA}$, $3.92 \pm 0.01 \text{ \AA}$, $3.87 \pm 0.01 \text{ \AA}$ and $3.88 \pm 0.01 \text{ \AA}$ for UL-Pt, UL-Au, UL-Cu and UL-Cr samples, respectively. XRD measurements have been performed between $2\Theta = 20^\circ$ and $2\Theta = 85^\circ$. No crystalline peaks for NiFe, IrMn, Cu and Cr textures are observable in the samples. Additionally, XRR measurements have been performed for the samples to characterize their thicknesses and interface roughnesses. The XRR data and theoretical simulation results for the samples are shown in figure 2b. Simulations were made by using Commercial Rigaku GlobalFit software. The data obtained by the simulations are compatible with the nominal values of the films and are given in Table I. Since the thicknesses of all layers in the samples are the same, the peak positions in the graphs seemed very similar especially up to $2\Theta=2^\circ$. It shows a consistency between the growth processes of all samples.

From the simulation data, it is calculated that the roughness values in the sample are relatively large. Since all elements used in sputtering systems can form alloys, these roughness values can be attributed to the interdiffusion of sputtered materials [30].

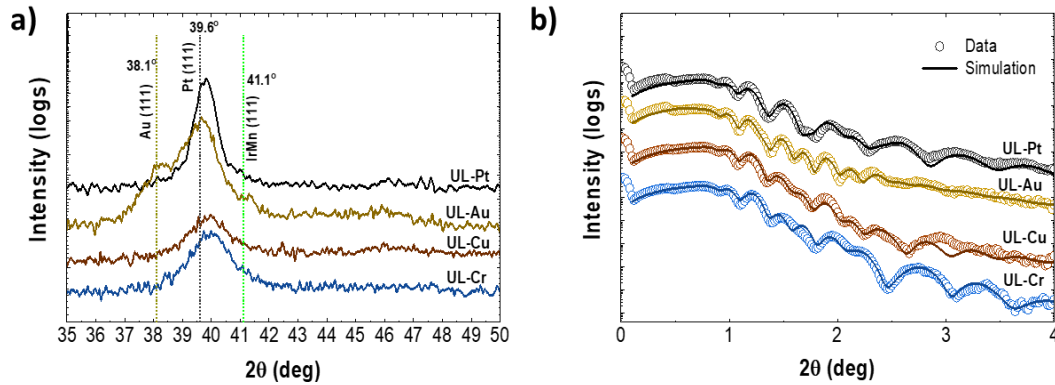


Figure 2. XRD patterns for the samples (a). The XRR data and theoretical simulation of the samples (b). Here in (b), open circles represent reflectivity data and lines indicate the fit of simulation data.

Table I. XRR simulation parameters for the samples.

Layer	Density [g/cm ³]	Thickness [nm]				Roughness [nm]			
		UL-Pt	UL-Au	UL-Cr	UL-Cu	UL-Pt	UL-Au	UL-Cr	UL-Cu
Si	2.33	-	-	-	-	-	-	-	-
<100>									
SiO ₂	2.64	500	500	500	500	0.81	0.393	0.92	1.046
	Au:19.3		5.51				1.47		
	0								
UL-x	Cr:			5.76				0.94	
	7.19								
	Cu:								
	8.96				5.235				1.78
Pt	21.10	13.48	8.59	7.84	8.16	0.25	1.75	1.64	1.71
Ni ₈₀ Fe	8.69	6.33	6.26	5.97	6.375	0.96	0.87	0.36	0.23
²⁰ Ir ₂₂ Mn	10.79	11.97	12.09	11.86	11.93	1.52	1.48	1.82	1.88
⁷⁸ Pt	21.10	3.21	2.98	2.88	3.235	1.42	1.59	1.79	1.83

Figure 3a-d shows the LMOKE hysteresis loops measurements at angles $\Phi_H = 0^\circ, 90^\circ$ and 180° for UL-Pt, UL-Au, UL-Cu and UL-Cr samples, respectively. As expected, $\Phi_H = 0^\circ$ and 180° seem to be the easy axis for all samples from their square-like hysteresis loops and $\Phi_H = 90^\circ$ seem to be the hard axis for all samples from their S-shaped hysteresis loops at that angle.

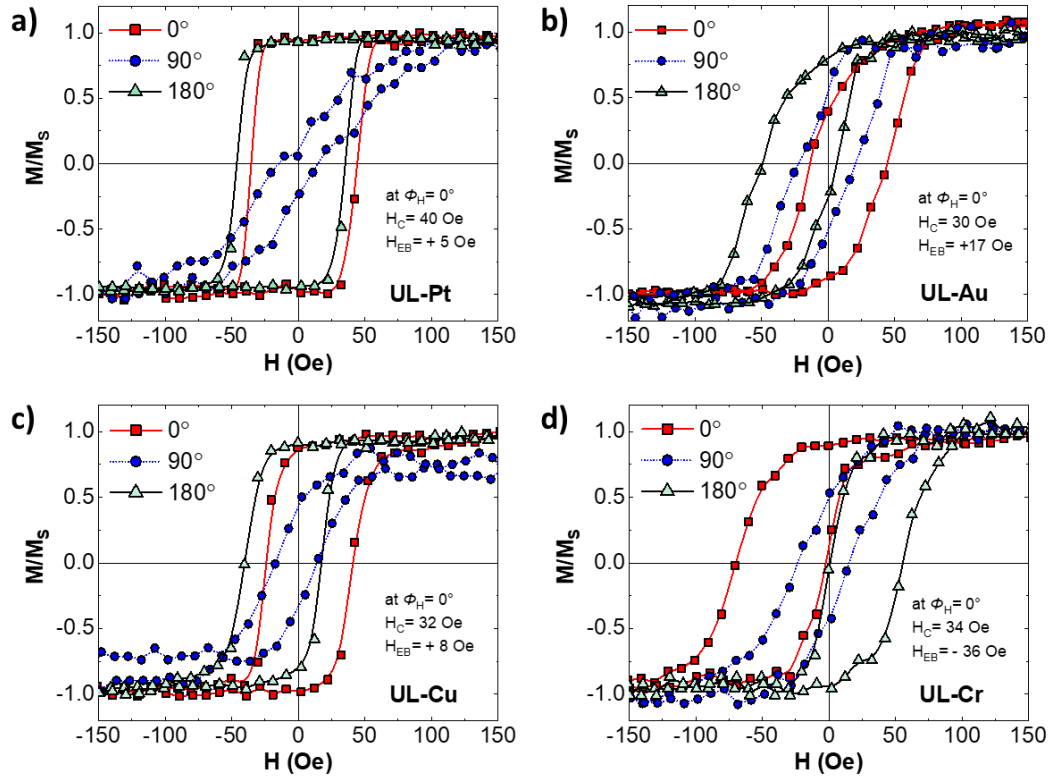


Figure 3. L-MOKE measurement results of (a) UL-Pt sample, (b) UL-Au sample, (b) UL-Cu sample and (c) UL-Cr sample.

It is noticeable from the $\Phi_H = 0^\circ$ angle measurements (solid squared dots) of figure 3a-d that the hysteresis loop shift value, which means H_{EB} , is larger in the UL-Cr sample than in the other samples. Moreover, the shift direction is to the negative values in the UL-Cr sample while the shift directions of UL-Pt, UL-Au and UL-Cu samples are to the positive values. These values were drawn in figure 4a to make a comparison between them. The coercive field (H_C) values varied from 40 Oe to 30 Oe depending on the type of UL. Exchange bias values (H_{EB}) are very low for the UL-Pt, UL-Au and UL-Cu which are +5, +17 and +8 Oe, respectively. However, UL-Cr has a larger H_{EB} value of -36 Oe and indicates a negative shift. Positive or negative values of H_{EB} in these results indicate a positive or a negative shift with respect to the reference axis ($\Phi_H = 0^\circ$) used in the measurements.

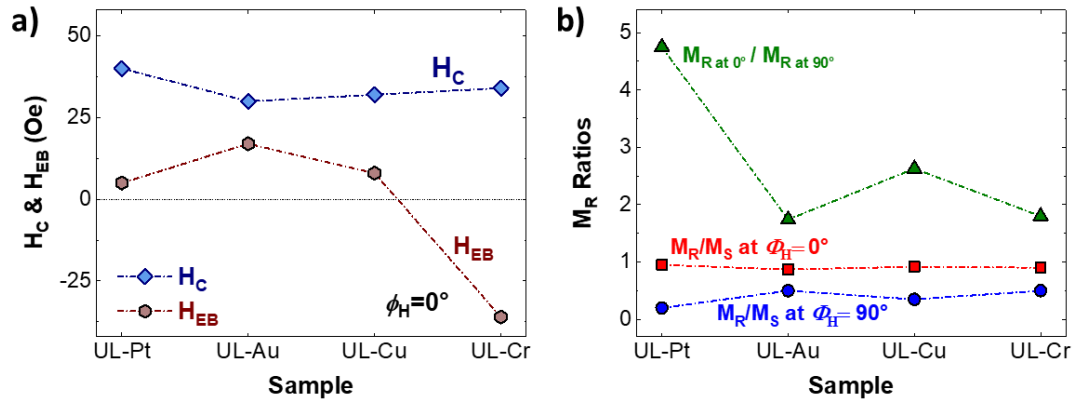


Figure 4. The comparisons of (a) H_C & H_{EB} values and (b) M_R ratios of the samples.

A UL can alter the crystal orientation, texture, microstructure, stress, or roughness in the layers of the stack. All these changes affect the total anisotropy of the ferromagnetic layer. Figure 4b is given to discuss the anisotropic behavior of samples. In the figure, M_R defines the remanent magnetization value and M_S defines the saturation magnetization value. M_R/M_S values at $\phi_H = 0^\circ$ are very close to each other for all samples and numerically the values are 0.95, 0.87, 0.90 and 0.92 for UL-Pt, UL-Au, UL-Cr and UL-Cu, respectively. At $\phi_H = 90^\circ$, M_R/M_S values are very different. They are 0.20, 0.51, 0.50 and 0.35 for UL-Pt, UL-Au, UL-Cr and UL-Cu, respectively. M_R/M_S values were also measured at other intermediate angles (not presented in the figures), and their results were found between these values. It can be concluded that all samples have easy axes at $\phi_H = 0^\circ$ and 180° and hard axes at $\phi_H = 90^\circ$ and 270° as expected. $M_{R-0^\circ} / M_{R-90^\circ}$ gives the remanent values rates of samples between their easy and hard axis. Among the samples, the UL-Pt sample has the highest value (4.75) which means that the UL-Pt sample is highly anisotropic compared to the other samples. The UL-Au sample has the lowest rate (1.74).

From the magnetic measurements, four distinct results of UL can be discussed. The varying ULs caused variations in (i) coercive field values, (ii) exchange bias values, (iii) exchange bias sign and (iv) magnetic anisotropies. The reasons for these differences in this study can be attributed to two main factors related to ULs. The first one is the UL's lattice parameters and crystalline structures, and the second one is the growth conditions. Bulk Pt (111) has a lattice parameter of 3.92 Å with a cubic close-packed (ccp) structure. Similarly, bulk Cu (111) and Au (111) have lattice parameters of 3.61 Å and 4.08 Å, respectively, with again ccp structures. However, Cr has a smaller lattice parameter of 2.91 Å with a body-centered cubic (bcc) structure. FM Py layer of the samples has the face-centered cubic (fcc) crystal structure with a lattice parameter of approximately 3.55 Å (for $Ni_{80}Fe_{20}$ [31]). After 5 nm ULs, the samples have 8 nm Pt layers. When the UL and Pt layer consistency of the samples are compared numerically in terms of lattice constants, it can be calculated that this ratio is 92% in the UL-Cu sample, 96% in the UL-Au sample and 75% in the UL-Cr sample. Cu, Au and Pt have similar kinds of crystal structures and have good lattice matches with high rates. UL-Cr sample has a lattice match with a lower rate, and it revealed significant differences in H_C and H_{EB} values. UL-Cr sample also caused a change in the direction of the EB effect and reduced the anisotropic character of the sample. For the UL-Pt and UL-Cu samples, the lattice match may be considered to explain the observation of similar magnetic properties. The only significant difference between the magnetic

properties of UL-Pt and UL-Cu samples was the presence of the highly anisotropic character of the UL-Pt sample. One can attribute this slight difference to their slight lattice mismatch. However, the results of the UL-Au sample do not have an agreement with this approach. Because, although there was a much better lattice match between UL-Pt and UL-Au samples (96%), they did not present similar results in terms of magnetic anisotropies, and H_C and H_{EB} values.

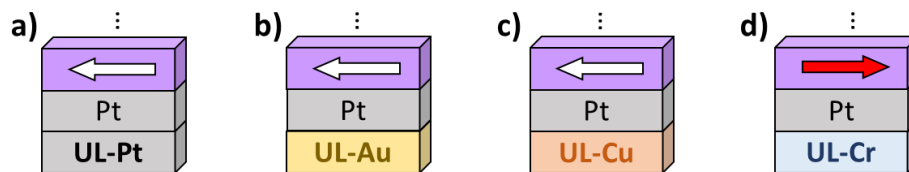


Figure 5. Magnetic moment orientation of (a) UL-Pt, (b) UL-Au, (c) UL-Cu and (d) UL-Cr samples.

The second approach to define the differences between the magnetic properties of samples is their growth conditions. Figure 5 illustrates the assumed initial positions of the magnetic moment (spin) directions of the samples which are responsible for the sign of EB. The figure means that the initial magnetic moment direction of the UL-Cr sample is in the opposite direction of UL-Pt, UL-Au and UL-Cu samples according to their initial measurement (and growth) position ($\Phi_H = 0^\circ$). The magnetic anisotropies should play a decisive role for these structures for their magnetic moment directions. It is previously found that the insertion of a buffer layer can change the morphology of the FM surface and the magneto crystalline anisotropy of the FM layer [25]. The MOKE data of the samples at 0, 90 and 180° indicates that samples have in-plane uniaxial magnetic anisotropy. This behavior of polycrystalline samples is explained by growth conditions. This type of anisotropy is called growth-induced or geometric (oblique) anisotropy [32, 33]. The growth conditions, i.e. the growth position of the target guns of the ULs, can alter growth-induced anisotropy and magnetoelastic energy. The total magnetic anisotropy differences in the samples can be the possible reason for the change in the EB direction. The gun positions were mentioned previously while defining figure 1b. From figure 1b, it can be said that all growth angles in the samples, except the growth angles of the ULs, are the same. The subsequent layer after the UL is non-magnetic Pt for each sample. Since Pt layers were deposited under the same conditions, the Pt layers in the samples must have indirect effects on the magnetic properties of the FM layers inherited from the growth conditions of ULs. The gun positions for Pt and Cu targets have almost the same orientation to the substrate (figure 1b), they are geometrically on the same line with the substrate, whereas the gun positions for Au and Cr are significantly different. This can explain why both UL-Pt and UL-Cu samples have higher anisotropic behavior than UL-Au and UL-Cr samples. However, despite these explanations, one question regarding the sign of EB still remains unanswered. In an exchange-biased system with a uniaxial FM anisotropy, two exchange coupling terms play important role in the total energy of an exchange coupled FM/AF bilayer [34]. These terms are called bilinear and biquadratic coupling energies. Normally, bilinear (direct) coupling between FM/AF layers has a dominating role in the exchange bias effect. On the other hand, the presence of 90° coupling between the magnetization of the FM/AF interface can be achieved in the samples with the help of biquadratic (or spin-flop) coupling. Both coupling energies can contribute to the EB effect in an FM/AF bilayer, and the value of their rate changes the value and sign of EB. These energy terms are strongly related to the grain size of the layer and the interdiffusions between the FM/AF layers. Here, the gun position of the Cr target is located at the opposite side of Py during the sample depositions. The position of Cr with the help of growth-induced anisotropy can give a rise to

changes in biquadratic and bilinear coupling energy terms. Additionally, the effect of the interface roughness cannot be excluded here. Roughness contributes to the observed changes in magnetic anisotropies and coupling energy terms. It also can contribute to the growth mode of the Py layer. The effect of roughness can generally be explained by the well-defined random field model of EB [35].

4. CONCLUSION

In summary, the role of Pt, Au, Cu and Cr underlayers on exchange bias properties in Pt/Py/IrMn thin films has been reported and discussed. It was found that the use of a thin Cr underlayer at the bottom was very effective in increasing the exchange bias field value of Pt/Py/IrMn multilayers and also in changing the direction of the EB effect. In contrast to what has been observed for the sample with the Cr underlayer, a very small EB effect is observed in the samples with Cu and Pt underlayers. The coercivity values in the studied samples slightly varied from 32 Oe to 40 Oe depending on the UL type. On the other hand, the exchange bias field values varied from +8 Oe to -36 Oe depending on UL type. Not the use of Cu or Pt, but the use of Cr as a UL has changed both the value and the sign of the exchange bias significantly.

This study can be extended with new samples by changing the UL target positions during the deposition for further research. The effect of underlayers is sometimes ignored as they were thought to be standardized for the multilayers, but our study once again revealed their importance in the design of magnetic multilayers by giving numerical results in EB value, EB sign and magnetic anisotropies. On this basis, one would expect that these results can play a significant role in designing new spintronic devices. This indirect effect of the underlayers on the magnetic properties may be potentially useful for further applications in technological devices since an underlayer can change the H_C values, H_{EB} values, EB sign and magnetic anisotropies to the desired value in the magnetic multilayers.

ACKNOWLEDGMENTS

We are grateful to the Nanomagnetism and Spintronics Laboratory (NASAM) of Gebze Technical University for the sputtering facilities provided for the sample growth. Magnetic measurements were performed at the MOKE and PPMS laboratories of the Physics Department of Gebze Technical University. The authors thank the staff member Adem Şen for his support during the XRD analysis.

REFERENCES

- [1] Baltz, V., Manchon, A., Tsoi, M., Moriyama, T., Ono, T. and Tserkovnyak, Y., (2018), Antiferromagnetic spintronics, *Reviews of Modern Physics*, 90, (1), 015005.
- [2] Železný, J., Wadley, P., Olejník, K., Hoffmann, A. and Ohno, H., (2018), Spin transport and spin torque in antiferromagnetic devices, *Nature Physics*, 14, (3), 220-228.
- [3] Meiklejohn, W. H. and Bean, C. P., (1956), New Magnetic Anisotropy, *Physical Review*, 102, (5), 1413-1414.

- [4] Demirci, E., Rojas, J. d., Quintana, A., Fina, I., Menéndez, E. and Sort, J., (2022), Voltage-driven strain-mediated modulation of exchange bias in Ir₂₀Mn₈₀/Fe₈₀Ga₂₀/Ta<011>-oriented PMN-32PT heterostructures, *Applied Physics Letters*, 120, (14), 142406.
- [5] Manchon, A., Železný, J., Miron, I. M., Jungwirth, T., Sinova, J., Thiaville, A., Garello, K. and Gambardella, P., (2019), Current-induced spin-orbit torques in ferromagnetic and antiferromagnetic systems, *Reviews of Modern Physics*, 91, (3), 035004.
- [6] Fang, B., San Jose, L. S. T., Chen, A. T., Li, Y., Zheng, D. X., Ma, Y. C., Algaidi, H., Liu, K., Finocchio, G. and Zhang, X. X., (2022), Electrical Manipulation of Exchange Bias in an Antiferromagnet/Ferromagnet-Based Device via Spin-Orbit Torque, *Advanced Functional Materials*, 32, (26).
- [7] Lin, P.-H., Yang, B.-Y., Tsai, M.-H., Chen, P.-C., Huang, K.-F., Lin, H.-H. and Lai, C.-H., (2019), Manipulating exchange bias by spin-orbit torque, *Nature Materials*, 18, (4), 335-341.
- [8] Zhang, J., Zhou, J., Luo, Z.-L., Chen, Y. B., Zhou, J., Lin, W., Lu, M.-H., Zhang, S.-T., Gao, C., Wu, D. and Chen, Y.-F., (2020), Exchange-biased nanocomposite ferromagnetic insulator, *Physical Review B*, 101, (1), 014422.
- [9] Wu, R., Xue, M., Maity, T., Peng, Y., Giri, S. K., Tian, G., MacManus-Driscoll, J. L. and Yang, J., (2020), Influence of atomic roughness at the uncompensated Fe/CoO(111) interface on the exchange-bias effect, *Physical Review B*, 101, (1), 014425.
- [10] Demirci, E., Öztürk, M., Pişkin, H. and Akdoğan, N., (2020), Angle-Dependent Inverted Hysteresis Loops in an Exchange-Biased [Co/Pt]₅/IrMn Thin Film, *Journal of Superconductivity and Novel Magnetism*, 33, (3), 721-726.
- [11] Dong, Y., Zhao, X., Wang, W., Chen, Y., Bai, L., Yan, S. and Tian, Y., (2022), Room temperature manipulation of exchange bias in magnetic heterojunctions, *Journal of Magnetism and Magnetic Materials*, 559.
- [12] Wu, H., Sudoh, I., Xu, R., Si, W., Vaz, C. A. F., Kim, J.-y., Vallejo-Fernandez, G. and Hirohata, A., (2018), Large exchange bias induced by polycrystalline Mn₃Ga antiferromagnetic films with controlled layer thickness, *Journal of Physics D: Applied Physics*, 51, (21), 215003.
- [13] Wang, R., Xiao, Z., Liu, H., Quan, Z., Zhang, X., Wang, M., Wu, M. and Xu, X., (2019), Enhancement of perpendicular magnetic anisotropy and spin-orbit torque in Ta/Pt/Co/Ta multilayered heterostructures through interfacial diffusion, *Applied Physics Letters*, 114, (4), 042404.
- [14] Ryu, J., Avci, C. O., Karube, S., Kohda, M., Beach, G. S. D. and Nitta, J., (2019), Crystal orientation dependence of spin-orbit torques in Co/Pt bilayers, *Applied Physics Letters*, 114, (14), 142402.
- [15] Zhu, L., Ralph, D. C. and Buhrman, R. A., (2019), Spin-Orbit Torques in Heavy-Metal-Ferromagnet Bilayers with Varying Strengths of Interfacial Spin-Orbit Coupling, *Physical Review Letters*, 122, (7), 077201.

- [16] Rowan-Robinson, R. M., Hindmarch, A. T. and Atkinson, D., (2018), Efficient current-induced magnetization reversal by spin-orbit torque in Pt/Co/Pt, *Journal of Applied Physics*, 124, (18), 183901.
- [17] Jinnai, B., Zhang, C., Kurenkov, A., Bersweiler, M., Sato, H., Fukami, S. and Ohno, H., (2017), Spin-orbit torque induced magnetization switching in Co/Pt multilayers, *Applied Physics Letters*, 111, (10), 102402.
- [18] Ramaswamy, R., Qiu, X., Dutta, T., Pollard, S. D. and Yang, H., (2016), Hf thickness dependence of spin-orbit torques in Hf/CoFeB/MgO heterostructures, *Applied Physics Letters*, 108, (20), 202406.
- [19] Skowroński, W., Cecot, M., Kanak, J., Ziętek, S., Stobiecki, T., Yao, L., van Dijken, S., Nozaki, T., Yakushiji, K. and Yuasa, S., (2016), Temperature dependence of spin-orbit torques in W/CoFeB bilayers, *Applied Physics Letters*, 109, (6), 062407.
- [20] Akyol, M., Alzate, J. G., Yu, G., Upadhyaya, P., Wong, K. L., Ekicibil, A., Amiri, P. K. and Wang, K. L., (2015), Effect of the oxide layer on current-induced spin-orbit torques in Hf|CoFeB|MgO and Hf|CoFeB|TaOx structures, *Applied Physics Letters*, 106, (3), 032406.
- [21] Engel, C., Goolaup, S., Luo, F. and Lew, W. S., (2017), Characterizing Angular Dependence of Spin-Orbit Torque Effective Fields in Pt/(Co/Ni)₂/Co/IrMn Structure, *Ieee Transactions on Magnetics*, 53, (11), 1-4.
- [22] Hayashi, M., Kim, J., Yamanouchi, M. and Ohno, H., (2014), Quantitative characterization of the spin-orbit torque using harmonic Hall voltage measurements, *Physical Review B*, 89, (14), 144425.
- [23] Cavicchia, D. R., D’Orazio, F., Rossi, L., Ricci, F. and Lucari, F., (2013), Influence of Cu seed layer on the magnetization reversal in exchange-biased FeMn/FeCo systems, *EPJ Web of Conferences*, 40, 13002.
- [24] Dunz, M. and Meinert, M., (2020), Role of the Ta buffer layer in Ta/MnN/CoFeB stacks for maximizing exchange bias, *Journal of Applied Physics*, 128, (15), 153902.
- [25] Ashida, T., Sato, Y., Nozaki, T. and Sahashi, M., (2013), Effect of the Pt buffer layer on perpendicular exchange bias based on collinear/non-collinear coupling in a Cr₂O₃/Co₃Pt interface, *Journal of Applied Physics*, 113, (17), 17D711.
- [26] Öksüzöğlü, R. M., Yıldırım, M., Çınar, H., Hildebrandt, E. and Alff, L., (2011), Effect of Ta buffer and NiFe seed layers on pulsed-DC magnetron sputtered Ir₂₀Mn₈₀/Co₉₀Fe₁₀ exchange bias, *Journal of Magnetism and Magnetic Materials*, 323, (13), 1827-1834.
- [27] Kohn, A., Kovács, A., Fan, R., McIntyre, G. J., Ward, R. C. C. and Goff, J. P., (2013), The antiferromagnetic structures of IrMn₃ and their influence on exchange-bias, *Sci Rep*, 3, 2412.

- [28] Nozières, J. P., Jaren, S., Zhang, Y. B., Zeltser, A., Pentek, K. and Speriosu, V. S., (2000), Blocking temperature distribution and long-term stability of spin-valve structures with Mn-based antiferromagnets, *Journal of Applied Physics*, 87, (8), 3920-3925.
- [29] Demirci, E., (2016), "Manyetoelektrik Cr₂O₃ Tabanlı İnce Film Sistemlerinde Dik Exchange Bias Etkisinin İncelenmesi [Investigation of perpendicular exchange bias effect in magnetoelectric Cr₂O₃ based thin films]", PhD Thesis, Written in Turkish, Gebze Technical University, Turkey.
- [30] Mokhtari, I. B.-E., Mourkas, A., Ntetsika, P., Panagiotopoulos, I., Roussigné, Y., Cherif, S. M., Stashkevich, A., Kail, F., Chahed, L. and Belmeguenai, M., (2019), Interfacial Dzyaloshinskii-Moriya interaction, interface-induced damping and perpendicular magnetic anisotropy in Pt/Co/W based multilayers, *Journal of Applied Physics*, 126, (13), 133902.
- [31] Li, G., Leung, C. W., Shueh, C., Hsu, H.-F., Huang, H.-R., Lin, K.-W., Lai, P. T. and Pong, P. W. T., (2013), Exchange bias effects of NiFe/NiO bilayers through ion-beam bombardment on the NiO surface, *Surface and Coatings Technology*, 228, S437-S441.
- [32] Knorr, T. G. and Hoffman, R. W., (1959), Dependence of Geometric Magnetic Anisotropy in Thin Iron Films, *Physical Review*, 113, (4), 1039-1046.
- [33] Özdemir, M., Aktaş, B., Öner, Y., Sato, T. and Ando, T., (1997), Anomalous anisotropy of reentrant Ni₇₇Mn₂₃ film, *J. Phys. Condens. Matter.*, 9, 6433-6445.
- [34] Hu, J.-g., Jin, G., Hu, A. and Ma, Y.-q., (2004), Temperature dependence of exchange bias and coercivity in ferromagnetic/antiferromagnetic bilayers, *The European Physical Journal B - Condensed Matter and Complex Systems*, 40, (3), 265-271.
- [35] Malozemoff, A. P., (1987), Random-field model of exchange anisotropy at rough ferromagnetic-antiferromagnetic interfaces, *Phys Rev B Condens Matter*, 35, (7), 3679-3682.